ACS OMEGA

http://pubs.acs.org/journal/acsodf

Article

Spontaneous Formation of Structures with Micro- and Nano-Scopic Periodic Ripple Patterns

Vijayendra Shastri, Santanu Talukder, Kaustav Roy, Praveen Kumar,* and Rudra Pratap

Cite This: *ACS Omega* 2022, 7, 12111−12119

Read Online

ACCESS | Metrics & More | Article Recommendations | Supporting Information

ABSTRACT: We report the first study on the formation of structures with micro- and nano-scopic periodic surface patterns created by the spontaneous flow of liquid metal over thin metallic solid films. Minute details of the flow of liquid gallium over gold are captured *in situ* at very high magnifications using a scanning electron microscope, and a series of experiments and microstructural characterization are performed to understand the underlying principles of the liquid flow and the pattern formation. This phenomenon is solely driven by wetting, with little influence of gravity, and is aided by a tenacious semi-solidus envelope of the intermetallic compound formed due to the reaction between the liquid metal and the metallic substrate. This complex flow creates highly periodic patterns with features ranging from hundreds of nanometers to tens of micrometers, which can be tuned *a priori*. We propose a model capturing the essential mechanics of the ripple formation and apply it to simulate the formation of a single ripple, along with its essential asymmetry, that forms the basis for generating the observed patterns.

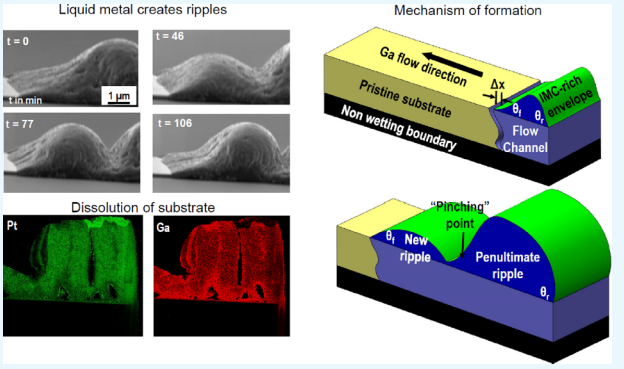

1. INTRODUCTION

Pattern formation is one of the fascinating characteristics of nature.[1] Specifically, liquid flow-driven patterns are observed at different length scales, varying from a few meters as in lava flow,[2] tidal bore,[3] etc., to a few tens of micrometers in the case of capillary waves.[4] Often the principles of fluid mechanics and thermodynamics are sufficient to understand the patterns created by nature; however, translation of the same principles at the lab as well as industrial scale to create patterns of practical importance remains challenging and an exciting endeavor. Hence, there remain only a few scientific studies on pattern creation at the micro- and nano-scale.[5,6] Here, we demonstrate and study the spontaneous flow of liquid metals, e.g., gallium (Ga) and tin (Sn), over thin solid films, e.g., platinum (Pt), gold (Au), etc., for continuous pattern generation at a small length scale. Like lava flow, which occurs at a large length scale, our study shows the formation of tunable wave-like structures by the liquid metal at a small length scale. Figure 1 demonstrates a few examples of the diverse patterns of Ga and Sn that, for the first time, are generated at a wide length scale, ranging from tens of micrometers to hundreds of nanometers. Realizing that the patterns shown in Figure 1 appear as "ripples", we phrase patterns produced as ripple patterns and the flow causing these patterns as ripple flow for ease.

Each ripple pattern shown in Figure 1 is created in a single step, with a high degree of repeatability, without requiring any special environment and dedicated instrumentation. On the contrary, creating three-dimensional patterns with sub-micrometer features requires high-end equipment, such as electron-beam lithography (EBL), in conjunction with multiple "masking-etching-writing" steps.[7,8] Furthermore, the features sizes, e.g., depth and width of trenches as well as the adjoining hills, can be varied over orders of the length scales (e.g., the trench width of hundreds of nanometers to tens of micrometers), and the patterns can be created over larger distances (e.g., a few micrometers to a few centimeters). Given this versatility and the potential application of these structures in the diverse fields of optics, sensing, microfluidics, die-printing, etc.,[9,10] we conduct this study to understand the mechanism of the formation of ripples. Previously studied techniques[11−16] show novel methods of producing patterns using liquid metals. However, a single-step process for creating patterns in ambient conditions with features ranging from 100 nm to 10 μm is not demonstrated in those studies. Compared to the study of the liquid flow over an inert substrate, whose modeling is relatively more straightforward,[17] the flow of liquid metal on the wetting and reacting substrate, as is the case of examples shown in

Received: January 18, 2022
Accepted: March 25, 2022
Published: April 3, 2022

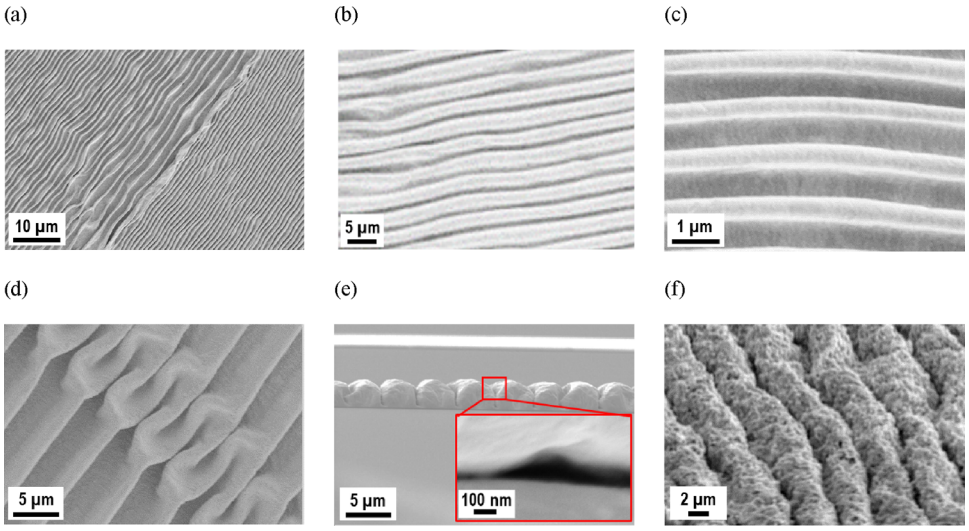

Figure 1. Micrographs, obtained using a scanning electron microscope (SEM), showing numerous prospects of the structures with periodic "rippled" surface patterns formed due to the spontaneous flow of liquid metals on solid metallic substrates (see Videos S1 and S2): patterns, with feature sizes ranging over 2 orders of magnitude, formed due to the flow of liquid (a–d) Ga on the Pt substrate, wherein the substrate is heated, (e) Ga on the Au substrate at room temperature, with the inset showing a feature at 10 times higher magnification, and (f) Sn on the Pt substrate at a temperature of 400 °C. All patterns shown here were created in ambient air conditions and in a single step. These are the first set of micrographs reporting metallic ripple structures at the micro- and nano-scale.

Figure 1, is complex. The added complexity is due to the solidification of chemically reacted species,[18] concentration gradient, and, at times, the oxidation of the liquid metal itself, potentially forming a thick and stiff envelope over the flowing liquid.[19] It should be noted that, although wetting of liquid Ga on thin films has been studied previously,[20,21] these studies neither discuss the ripple flow nor present the mechanism of the formation of the ripple patterns. Rather, the previous studies focused on the aspects like the formation of nanoneedles of Ga and the mechanism of synchronized spreading of Ga on thin films. To the best of our knowledge, this is the first study dedicated to the formation of the ripples and its mechanism.

2. EXPERIMENTAL PROCEDURE

For gaining insights into the steps of ripple formation, we perform experiments inside an SEM. Hence, for simplicity (related to heating, vapor pressure, contamination of chamber, etc.), we choose to perform a detailed study on liquid Ga, even though the formation of ripple patterns is not limited to this system (e.g., see Figure 1f). The sample configuration, with the relevant dimensions, is schematically illustrated in Figure 2a. For a given experiment, the width, thickness, and type (Au or Pt) of the thin film metal track are constant. The thickness of the Au film varies in the range of 150–300 nm for different samples, whereas the Pt film is in the range of 150 nm to 2 μm. The thickness of Pt is kept slightly higher than that of Au because the subsequent characterization involves focused ion beam (FIB) milling, which damages very thin Pt films. The top view of the sample after the photolithography and the subsequent thin film deposition is shown in Figure 2b. The width of the narrower region of the metal track in the sample, wherein the flow behavior is studied *in situ*, varies in the range of 4–35 μm. This sample configuration ensures the flow to be one-dimensional, which is relatively easy to analyze and understand.

Subsequently, a droplet of Ga with a diameter of ∼600 μm is placed manually on the wider section of the metal-film

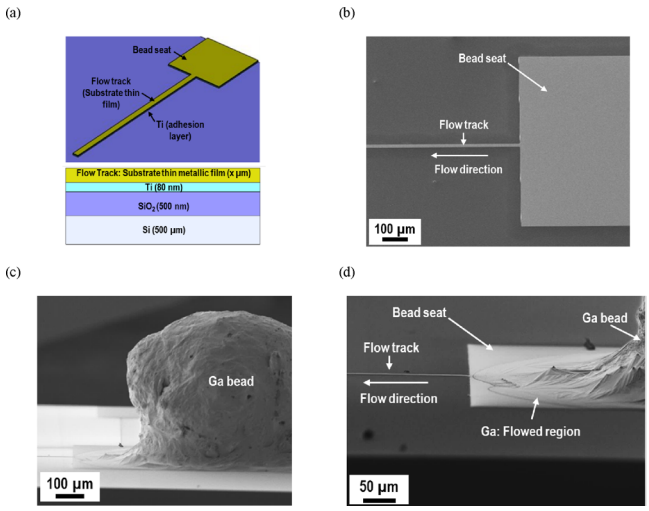

Figure 2. Specifics of the experimental procedure used to study the formation of the ripple patterns on a metallic substrate (i.e., track): (a) schematic illustration of the sample and SEM micrographs showing (b) the top view of the metal track over which liquid Ga flows, (c) side view of the Ga bead sitting on the wider section of the metal track (also named as the "bead seat"), and (d) side view of the flow of Ga from the wider section (i.e., bead seat) to the narrow region.

substrate (Figure 2c). Ga wets both Au and Pt at room temperature, with both Ga-Pt[22] and Ga-Au[23] systems having stable intermetallic compounds (IMC) at room temperature. However, for forming good contact with the substrate film, Ga is heated to ∼100 °C for a short time before the start of the *in situ* experiment inside an SEM. There is no hard rule on heating to a temperature of 100 °C. Heating at 50 °C will also suffice the contact establishment process, however, at a slower rate. Once Ga is molten, it starts to flow over the metal track through the "open channel" (see Figure 2d).[a] More details of the experimental procedure and imaging can be found in Section S1.

https://doi.org/10.1021/acsomega.2c00364
ACS Omega 2022, 7, 12111–12119

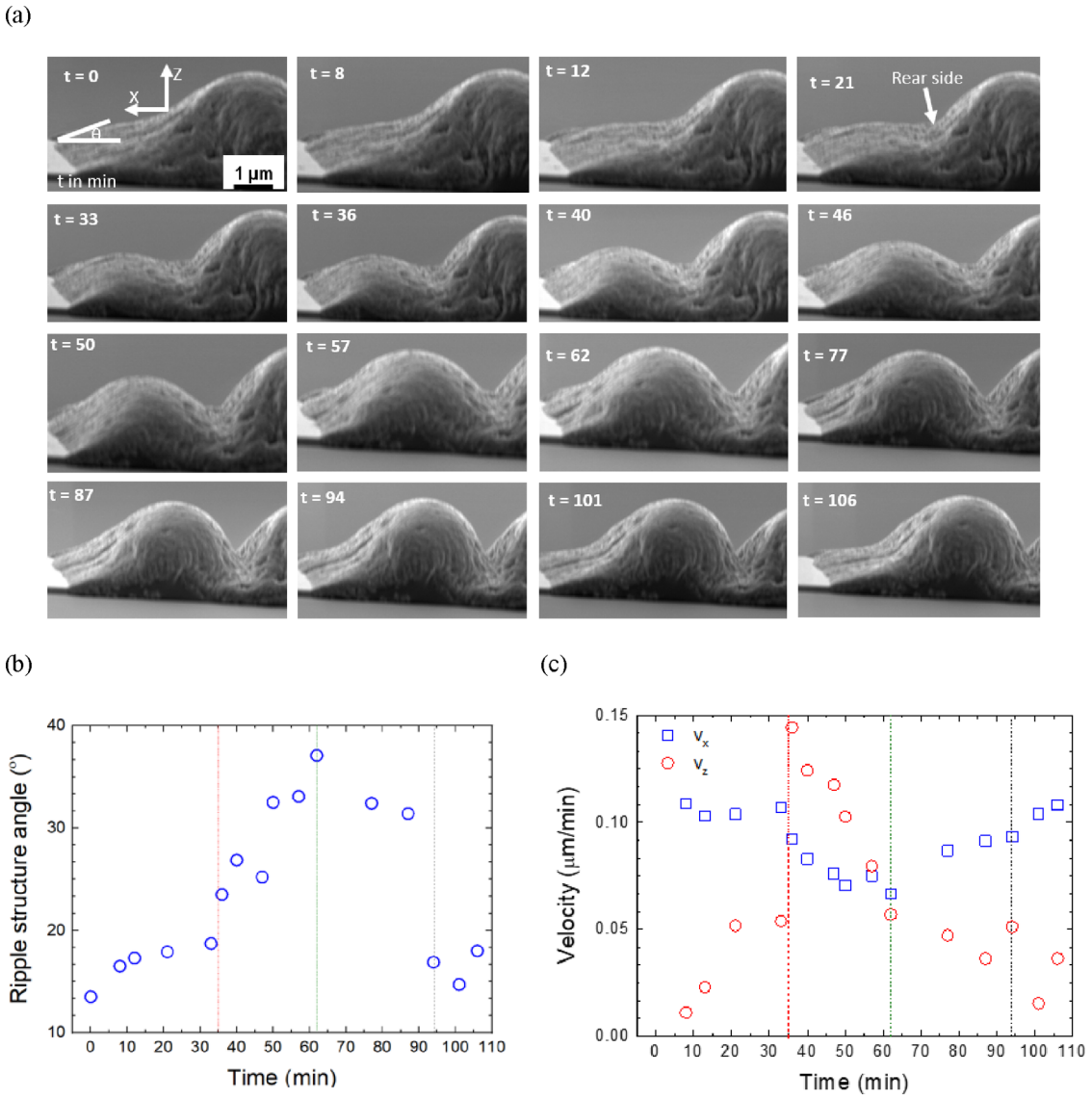

Figure 3. Tracking and quantifying nucleation and growth of the ripple structure: (a) time-lapse micrographs showing the evolution of the shape of ripples as liquid Ga flows over the Au thin film. The timestamp (t), in minutes, is shown in each micrograph. The definitions of the ripple structure angle and the coordinate system are given in the left-top micrograph. Variation of (b) the ripple structure angle and (c) forward flow velocity, v_x, and thickening rate, v_z, with time. The time axis in all figures shown here is synchronized with each other.

3. RESULTS: UNDERSTANDING THE RIPPLE STRUCTURE

3.1. Nucleation and Growth of the Ripple. The nucleation and growth of the ripple structure are shown in Figure 3a through a series of time-lapse micrographs (see Videos S1 and S2 for the ripple formation). Figure 3a reveals that, as the flow front of Ga advances, the shape of the ripple structure continues to evolve during the formation of successive ripples. The acute angle formed by the tangent drawn with the horizontal, as shown in the schematic (in the t = 0 min micrograph of Figure 3a), is used to characterize the evolution of the ripple shape as it forms and grows. We call this angle the ripple structure angle, whose variation with time is shown in Figure 3b. The ripple structure angle gradually rises initially as the liquid metal moves forward followed by a rapid increase and then a sharp decrease such that the ripple structure angle varies in the range of 14−40° from the start to the time the ripple remains at the front. It should be noted that this drop in the angle is associated with the front surface of the ripple. The rest of the structure, which is behind the flow front (e.g., rear side in the t = 21 min micrograph in Figure 3a), keeps evolving above 40°, till about 100−110°, with the horizontal. The fall in the ripple structure angle is attributed to the beginning of the "pinching" of the ripple, which is defined as the nucleation of the ripple at the front (see the micrograph corresponding to t = 94 min in Figure 3a, where the process of pinching is complete throughout the width of the ripple pattern). This cycle of the increase in the ripple structure angle followed by a decrease in between two successive pinching events continues throughout the ripple flow.

The growth of the frontmost ripple structure is observed in both the x and z directions (see Figure 3a for the definition of x and y coordinates). The corresponding velocity measurement is performed by post-processing of the recorded images using open-source software, called ImageJ, and shown in Figure 3c. The forward flow velocity, v_x, is very low, in the order of 1−3 nm/s, and is in the laminar regime with Reynolds number, *Re*

https://doi.org/10.1021/acsomega.2c00364
ACS Omega 2022, 7, 12111−12119

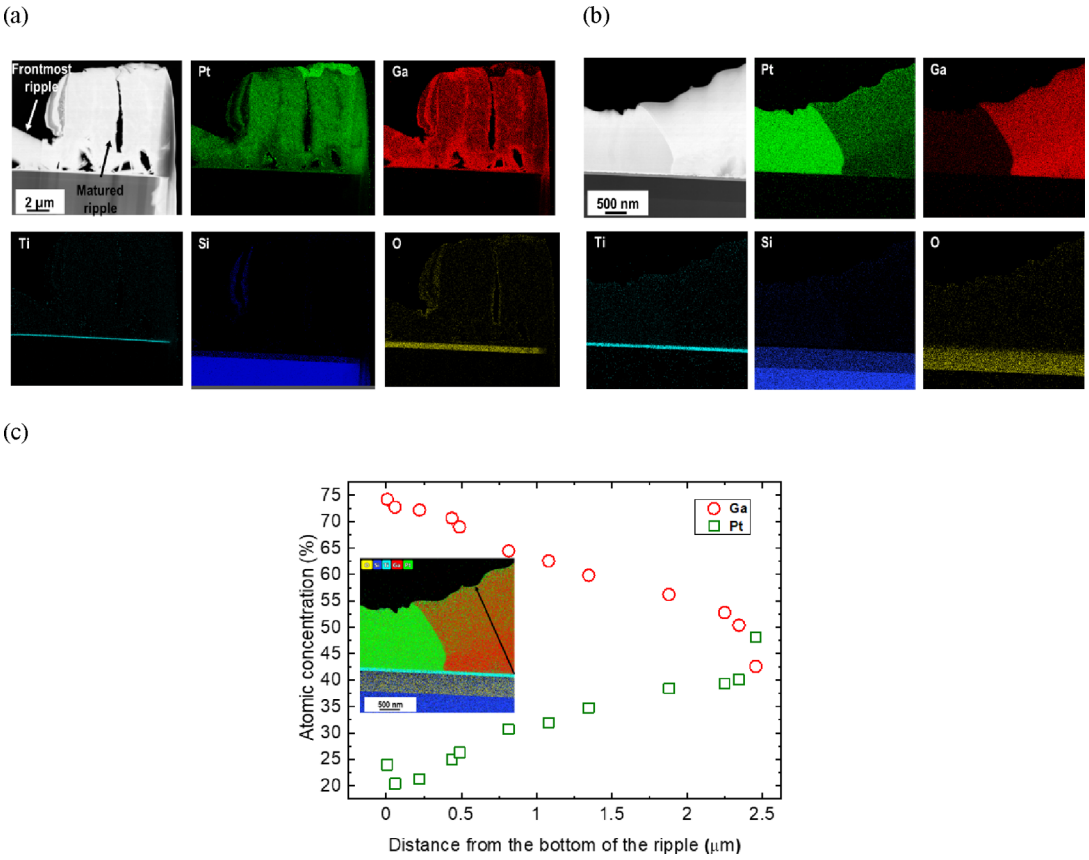

Figure 4. Elemental analysis of the ripple pattern using EDS in STEM: (a) matured (or penultimate) as well as some parts of the frontmost and (b) yet evolving ripple structure. The left top is the HAADF micrograph of the ripple structure, whereas the rest of the micrographs show the compositional map of the relevant elements. The name of the elements is mentioned in each map. (c) Variation of the average atomic concentration of Ga and Pt on the visible (i.e., side) surface as a function of the distance from the bottom of the ripple structure, along the arrow shown in the inset. The inset shows superimposed EDS color maps of all major elements.

$\ll 1$ (as shown later, $\sim 10^{-12}$). Furthermore, v_x starts with a higher value and gradually decreases to a smaller value before it starts to rise again. On the other hand, the velocity in the z direction or thickening rate, v_z, starts with a lower value and rapidly rises to a very high value before decreasing again to a very low value.

Three vertical lines are drawn in Figure 3b,c, denoting three important events during the nucleation and growth of a ripple structure. The first or the leftmost line denotes the event of the start of clear separation between the frontmost and the penultimate ripples (see micrographs corresponding to t = 21 and 33 min in Figure 3a): This leads to a rapid increase in the ripple structure angle (as if the substrate-liquid metal wetting has worsened), a sudden jump in v_z (or thickening rate), and a decrease in v_x. The second vertical line represents the event of localized pinching, i.e., nucleation of the new ripple at the flow front (see the micrograph corresponding to t = 62 min in Figure 3a, which shows a change in curvature). This leads to a decrease in the ripple structure angle (as if the liquid is now moving over a wetting layer) and a corresponding increase in v_x (i.e., the spread of liquid over the substrate) and a decrease in v_z. The third or rightmost line represents the completion of pinching over the entire width of the ripple front (see the micrograph corresponding to t = 94 min in Figure 3a), thereby completing the nucleation of the new ripple. At this instance, a sudden decrease in the ripple structure angle is observed, whereas v_x and v_z continue to increase and decrease, respectively.

Interestingly, v_x does not reduce to zero at any instant of the flow, implying that the flow front keeps moving, however, at a much slower rate during which the ripples thicken. Once a single ripple structure attains equilibrium, liquid Ga continues to flow beneath the structure without affecting the already formed ripple. The ratio of the height to width of the ripple structure is ≈ 1, with the average height lying within 3−8 μm, depending on the width of the track (see Section S2).

In summary, the nucleation of the ripple is identified as a combination of a small ripple structure angle, a faster spreading rate of the flow front, and a sluggish rate of thickening. On the other hand, the growth of the ripple involves an increase in the ripple structure angle and an associated preferential thickening (as compared to spreading).

3.2. Elemental Characterization. The very first question in our quest for understanding the ripple formation is about the chemical composition of the ripple structure. As per the phase diagram, Ga reacts with the substrate thin film (Au or Pt) and forms an intermetallic compound. Hence, it is essential to understand the evolution of the chemical composition of the ripple structure to gain critical insights into the mechanism of the ripple formation. The chemical composition of the ripple structure is examined using energy-dispersive spectroscopy (EDS) in scanning transmission electron microscopy (STEM). For performing EDS using STEM, a lamella of the ripple

https://doi.org/10.1021/acsomega.2c00364
ACS Omega 2022, 7, 12111−12119

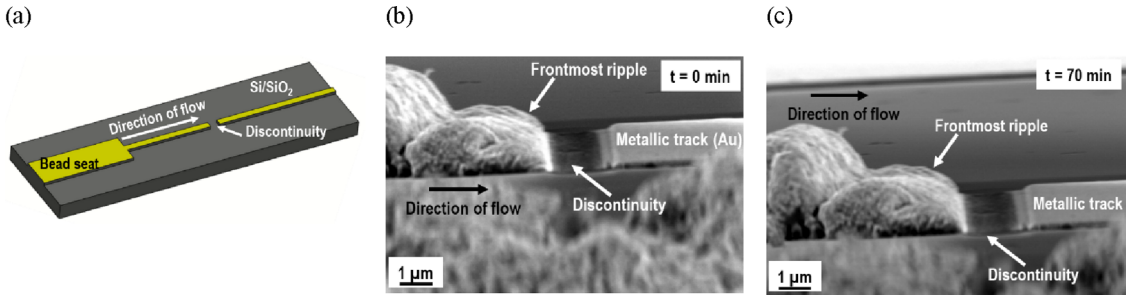

Figure 5. Evolution of the shape of the ripple on a discontinuous metallic track: (a) schematic illustration of the sample with a discontinuity in the flow track and SEM micrographs showing the ripple flow on a discontinuous Au metallic track at the time (b) when the flow front reaches the discontinuity (i.e., t = 0 min) and (c) after a further wait of 70 min (i.e., at t = 70 min) relative to the instance shown in panel (b) (see Video S3).

structure was fabricated using FIB milling. For fabricating Ga-on-Pt lamella, a 2 μm-thick ripple flow sample comprising one fully formed ripple and a half-formed ripple (see Figure 4) is milled using FIB and then thinned down to 200 nm thickness using very low currents (0.79 nA−2.5 nA). The lamella is lifted and placed onto a TEM grid (made of Cu).

Now, a close inspection of Figure 4, which shows the elemental maps of the matured (i.e., penultimate) ripple and the frontmost ripple, reveals the following:

- Pt is distributed throughout the ripple pattern, suggesting its complete dissolution during the liquid Ga flow.
- The distribution of Ga is limited to only the ripple pattern (or the flowed region), which confirms limited contamination of the sample due to FIB milling using Ga ions.[b]
- Ga does not diffuse below the titanium (Ti) adhesion layer, i.e., Ti acts as an excellent barrier layer for Ga, and hence, Ti is not a part of the ripple structure. The integrity of the Ti layer is preserved. It should be noted that Ga does not wet Ti (as revealed in an experiment dedicated to observing wetting of Ga on Ti, see Section S3), and hence, dissolution of Pt brings liquid Ga in direct contact with a non-wetting layer.
- Similar to Ti, silicon (Si) and silicon dioxide (SiO_2) are also not wetted by Ga and hence do not become a part of the ripple pattern. Their integrity is preserved throughout the ripple flow.
- Oxidation of the top layer of the ripple pattern is insignificant. A dedicated experiment performed to ascertain the role of oxygen (O) in the ambient confirms that oxidation does not play a role in the ripple flow (see Section S4).
- As discussed above, EDS-STEM analysis suggests the important role of dissolution of Pt (or the metal path) in liquid Ga and exposure of liquid Ga over a non-wetting Ti layer as essential aspects of the ripple flow. Remarkably, Figure 4c confirms dissolution and spread of Pt throughout Ga, with Ga and Pt being richer and leaner, respectively, at the bottom of the ripple pattern (i.e., closer to the Ti layer). This suggests that Ga might have been in purer form at the bottom of the ripple flow, maintaining a fully liquid channel for the flow toward pristine Pt (or the metallic path). On the other hand, the almost equiatomic concentration of Ga and Pt near the top surface of the ripple suggests the formation of a Ga-Pt intermetallic compound, which would provide a relatively stiffer envelope to liquid Ga flowing underneath.

3.3. Ripple Flow over a Discontinuous Track. Material characterization reveals the dissolution of the wettable substrate thin-film track and the exposure of the non-wetting, impervious Ti layer at the bottom. This confirms the important role of wetting, and on this basis, we try to understand the primary driving force behind the phenomenon. In this regard, an experiment is carried out by observing the liquid metal flow on a metallic track with a discontinuity at a certain distance from the start of the flow. A schematic of the experimental setup is illustrated in Figure 5a, and Video S3 shows the flow of liquid Ga over such a track. Figure 5b and Figure 5c show the frontmost ripple once the flow front reaches the discontinuity and after a long time of its arrival at the discontinuity, respectively. Figure 5 clearly reveals that flow seizes with no considerable change in the already formed ripple structure once the flow front reaches the discontinuity (i.e., when the wettable substrate is no longer available). It should be noted that the regular ripple structure formed (similar to that shown in Figure 3a) until the liquid metal front reached discontinuity. This implies that the continuation of liquid metal flow, the formation of the ripple structure, and evolution in the ripple structure depend on the wetting of the metallic track in the liquid metal: The movement in both the x and z directions requires a moving front. Hence, the ripple flow occurs due to a "pull-force" applied on the liquid metal front by the wettable metallic track and not due to any "push-force" that might arise due to a built-up of the hydrostatic pressure behind the flow front (e.g., due to the liquid metal placed on the bead seat, penultimate ripple structure, etc.). In other words, the surface tension between the solid thin film and liquid Ga, giving rise to a pull-force at the front, is the driving force for the flow.

4. DISCUSSION: MODELING RIPPLE FORMATION

As mentioned earlier, the ripple flow pattern involves a wetting-driven flow of the liquid metal and the dissolution of the substrate into the flowed metal. Comprehensive quantitative modeling of this phenomenon is beyond the scope of the current work; however, a qualitative model, based on the aforementioned experimental observations, is presented here that captures the essential features of the phenomenon. First, we present a qualitative interpretation of forces involved in this phenomenon and then describe a computational model based on finite element-phase field analysis that we use in commercial software, COMSOL Multiphysics, to study the ripple formation.

https://doi.org/10.1021/acsomega.2c00364
ACS Omega 2022, 7, 12111−12119

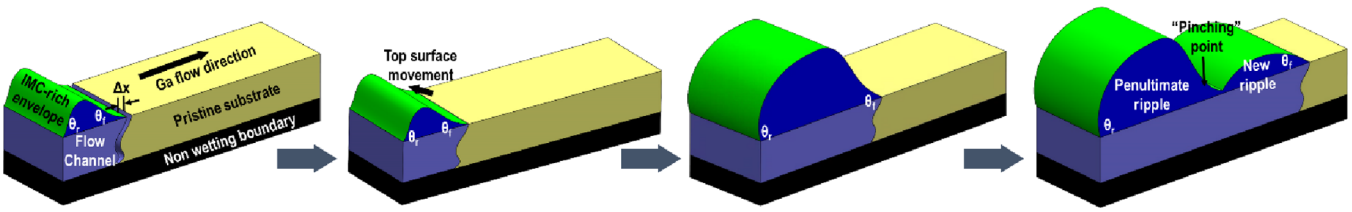

Figure 6. Schematic illustration of the sequences, involving wetting and dissolution of the metallic path, formation of the intermetallic compound (IMC) or substrate metal-rich envelope on the top surface, pulling forward of liquid due to wetting and its spheronization (due to the non-wetting layer at the bottom and surface tension of the liquid), and pinching of the ripple, leading to the formation of the ripple flow pattern. The steps of the ripple flow go from the left to the right in the above schematics. θ_r and θ_f are the ripple structure angles between the liquid and the substrate at the back and frontmost ends of a ripple, respectively.

4.1. Identification of the Dominant Driving Force. Surface tension between different interfaces involved in the ripple flow is expected to play a key role in ripple formation. To understand the relative significance of surface tension, γ, and body force (i.e., gravity), the capillary length, λ_c, is calculated as[24]

$$\lambda_c = \sqrt{\frac{\gamma}{\rho g}} \tag{1}$$

where ρ and g are the density of liquid metal and the gravitation acceleration, respectively. For pure Ga (with ρ = 6085 kg/m^3, γ = 722 mN/m, and g = 10 m/s^2),[25,26] λ_c is 3.3 mm. The length scale of a single ripple (e.g., <10 μm) is significantly smaller than the calculated capillary length, and hence, its size is not determined by the body forces. In other words, the hydrostatic pressure (in tens of Pa) is less than the Laplace pressure (in hundreds of KPa) generated due to the curvature. Hence, the role of gravity in ripple formation can be neglected, which is consistent with the experimental observations (see Section S5).

In the same context, the significance of the surface tension with respect to the viscous force can be estimated using the capillary number, C_a, which is the ratio of viscous force to surface tension force and is given as[27]

$$C_a = \frac{\mu v}{\gamma} \tag{2}$$

where μ represents the dynamic viscosity[25] and v is the velocity of flow. The capillary number for the flow is of the order of $\sim 10^{-9}$, clearly suggesting an insignificant role of viscosity relative to surface tension in the ripple flow. Furthermore, the Reynolds number, Re, which is the ratio of the inertia force to viscous force, is given by the following expression for a rectangular cross section[28]

$$Re = \frac{Dv}{\mu} \tag{3}$$

where D is the hydraulic diameter, given as $D = 4A/P$, where A and P are the cross-sectional area and the perimeter of the channel, respectively. The Reynolds number for the liquid Ga flow on Pt or Au is $\sim 10^{-12}$, which suggests a negligible role of inertia force relative to the viscous force. Hence, based on the values of λ_c, C_a, and Re, it can be concluded that surface tension (and hence wetting) plays the dominant role in the ripple flow, relative to the gravitational, viscous, and inertial forces. Hence, a model for this flow must incorporate the fact that the flow is primarily driven by interface forces that try to minimize the surface area.

4.2. Steps Leading to Ripple Formation. The surface tension-driven tendency of a liquid to minimize the surface area for a given volume at any given instance leads to the "spheronization" of liquids and semi-solidus materials. Based on this idea, a probable sequence of events involved in the formation of the ripple pattern can be conceived, as illustrated schematically in Figure 6. Here, the liquid metal moves over the metallic path driven by the surface wetting (see Figure 5). As an incremental portion of the substrate metallic path ("Δx" in Figure 6) is wetted by the liquid and dissolved into it, a thin layer of an intermetallic compound is formed, which ends up forming the top solidified surface (see Figure 4). The incremental length of the intermetallic compound layer is connected to the previously formed layer of the intermetallic compound; however, the newly formed layer is not yet fully solidified. This liquid spreading and metallic path dissolution lead to the pulling of additional liquid from the reservoir (see Figure 6); however, the newly arrived liquid in the ripple is now exposed to a non-wetting surface (i.e., Ti layer at the bottom, see Figure 4). This leads to upward pushing of the liquid and its spheronization, with a contact angle for the "sphere" at the bottom interface equal to 110 ± 4°, which is the equilibrium contact angle between the liquid Ga and Ti (see Section S3). This is further aided by the inherent tendency of the liquid to minimize its surface area by adopting a spherical or curved shape. As the top layer of the intermetallic compound is not completely solidified, the Laplace pressure applied on it (due to the surface tension of the liquid) deforms it, resulting in a distinct ripple shape, as observed in Figure 3a.

As shown in Figure 6 and observed from *in situ* experiments (Figure 3), the ripple structure angle between the incipient ripple and the substrate continuously increases, during which the ripple grows in its size. The size growth gives the ripple pattern a convex shape, indicating that the pressure inside the ripple is not only higher than the atmospheric pressure but also it is high enough to deform (and shape) the semi-solidus intermetallic compound layer. This pressure also acts against the flow of the liquid metal coming from the liquid reservoir to the ripple, and hence, the addition of the liquid metal into the ripple will stop if the pressure reaches a critical value. However, if this pressure is large enough to open a larger "orifice" at the flow front, then the liquid can ooze out to the pristine metallic surface at a faster speed, which can lead to nucleation and growth of a new ripple. The nucleation of a new ripple is associated with a pinching event, as schematically shown in Figure 6. The pinching event corresponds to the deepening of the top surface at a location a little behind the flow front (see Figures 3 and 6). The surface experiencing this pinching event

https://doi.org/10.1021/acsomega.2c00364
ACS Omega 2022, 7, 12111−12119

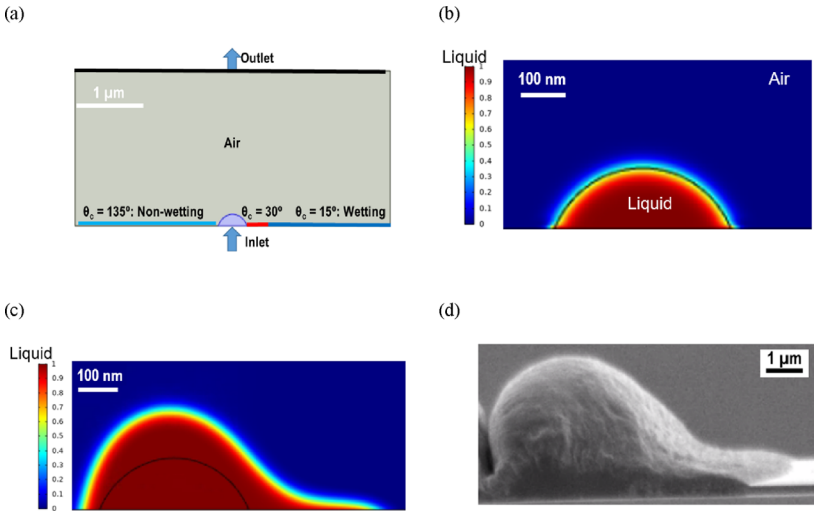

Figure 7. Numerical simulation capturing the liquid metal flow driven by wetting with asymmetric boundary conditions, leading to the formation of a typical ripple: (a) schematic of the COMSOL model (see Section S7 for details), (b) volume fraction color map at the initial time (i.e., t = 0 s), (c) volume fraction color map after the lapse of some time (here, t = 32 s), and (d) an SEM micrograph of a representative ripple showing the typical asymmetric shape of the ripples. The red-brown and blue colors in panels (b, c) represent the liquid (1 in color code) and air phases (0 in the color code), respectively, whereas the region in between these two pure phases is the interface region (as the boundary between these two phases is selected to be diffused in the COMSOL phase-field module) (see Video S4 for the simulation results).

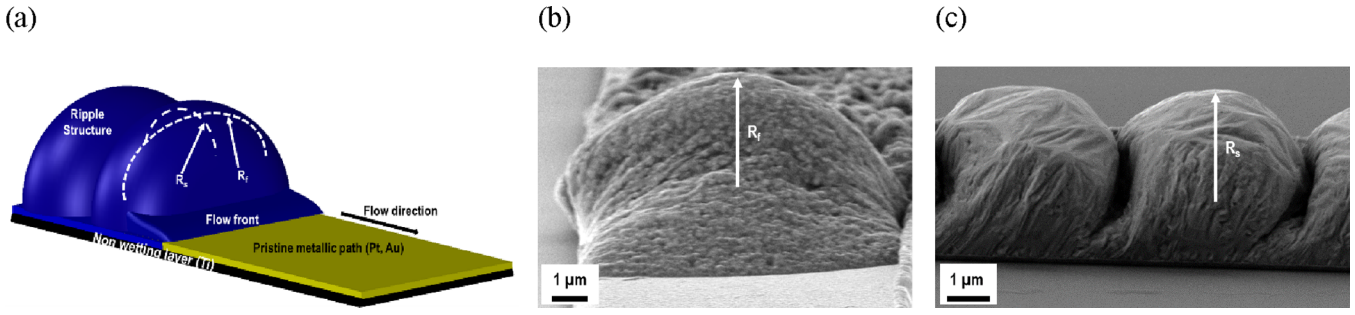

Figure 8. Measurement of the principal radii, R_s and R_f, of a ripple pattern: (a) 3D schematic showing the ripple structure, flow front and the definitions of R_s and R_f, and the method implemented for measuring (b) R_s and (c) R_f using appropriate SEM micrographs of a ripple.

continues to deepen, resulting in eventual separation between the penultimate ripple and the incipient ripple at the front of the flow. It should be noted that the process of formation of the intermetallic compound, which eventually provides a relatively stiff and hence stable top surface of the ripple pattern that experiences the pinching, is a continuous process as long as the flow front is not interrupted.

4.3. Simulating Ripple Flow and Evolution of Its Shape: Growth of the Ripple. A 2D model is built in COMSOL Multiphysics, wherein a liquid pool is introduced from an orifice at a constant velocity using the inlet boundary conditions (see Section S7 for details of COMSOL modeling). At one end of the orifice, the substrate is non-wetting (imitating the region where liquid metal is exposed to the non-wetting Ti layer), whereas the other end of the orifice has a small segment of a moderately wetting boundary (imitating the region where some Pt or Au is still partially left) followed by a wetting boundary (imitating the region where pristine Pt or Au exists, i.e., where the liquid has still not reached) (see Figure 7a). The top region is occupied by a compliant air medium. Interestingly, as shown in Figure 7b,c, the liquid drop starts to flow toward the wetting substrate and transitions from a relatively spherical shape to a slightly asymmetric shape (elongated toward the wetting region) (see Video S4). Thus, the existence of the asymmetric boundary conditions leads to the forward flow of the liquid and creates asymmetry in the shape of the ripple pattern. These predictions match well with the experimental observation (see Figure 7d). This simple qualitative computational model strongly suggests wetting to induce the liquid metal flow in the forward direction and the transition of the bottom layer from the wetting one (i.e., when Pt is there) to the non-wetting one (i.e., when Pt is dissolved, thereby exposing the liquid to Ti) to be responsible for its unique shape. This type of asymmetric shape is also discussed previously,[29] where a constant volume of a water droplet is placed over a surface, with one side being hydrophilic and another being hydrophobic.

4.4. Modeling Pinching Event: Nucleation of the Ripple. Liquid tries to minimize its surface area for a given volume. The volume of liquid keeps increasing due to the moving front, which adds more and more liquid to the ripple structure. The addition of a new volume of liquid and the presence of dewetting boundary at the bottom change the shape of the ripple structure continuously. There is a moving front and non-moving end at the sides of a ripple. The angle at the non-moving end continuously increases toward its equilibrium contact angle (110° approximately, with Ti). The ripple structure angle at the moving front increases to a

https://doi.org/10.1021/acsomega.2c00364
ACS Omega 2022, 7, 12111−12119

limit and then decreases. The decrease is attributed to the event of pinching. The addition of new liquid to the structure ceases and forms a new ripple after pinching. The limiting factor in the case of pinching is the surface tension of the structure. The surface tension of the ripple structure is different from actual Ga due to the intermetallic formation. The maximum amount of liquid added depends on the surface tension and thereby Laplace pressure resulting from surface tension. A simple analysis based on the Laplace pressure is performed to explain the conditions responsible for the nucleation of the new ripple. An estimate for the pressure at which the pinching event occurs can be qualitatively estimated by considering the Laplace pressure. Laplace pressure, which signifies the pressure difference across an interface, ΔP, is given[27]

$$\Delta P = \gamma\left(\frac{1}{R_f} + \frac{1}{R_s}\right) \quad (4)$$

where R_f and R_s are the principal radii of curvature of a ripple measured from the front and the side, respectively (see Figure 8). SEM micrographs are used to measure R_f and R_s at the moment when pinching or nucleation of a new ripple typically occurs (see Figure 8b,c). The typical values of R_f and R_s observed in this study vary between 2 and 5 μm. These values result in a Laplace pressure of 250−470 kPa between air and ripple, which is high for a non-solid enclosure. Since the primary force of driving is a pull-force at the front, the liquid addition prefers to create a new surface by moving forward (and hence pinching) rather than the bursting of the ripple.

It should be noted that the principal radii of curvature of the ripple decrease with an increase in the ripple size (given that liquid Ga reaches a non-wetting layer of Ti), and hence, the Laplace pressure increases with the height of the ripple. This leads to an increase in the force applied, and hence, its tendency of exceeding the surface tension increases with the height of the ripple. Thus, the pinching event or nucleation of the new ripple occurs only after the ripple has attained a certain height.

Although the phenomenon of ripple pinching is wide open for better modeling, we have reported our current understanding based on the experimental evidence described above. We also model the pinching part using the features currently available in COMSOL Multiphysics. Details of this model can be found in Section S6.

5. CONCLUSIONS

We have demonstrated and studied a novel patterning process using the spontaneous flow of liquid metals over metallic tracks at micro- and nano-scales. As mentioned earlier, no study till now has explored the mechanism of the formation of the ripple formation and it has not been touched upon in the relevant previous works.[20,21] The pattern formation reported here is unique because, till now, studies have shown wrinkles or waviness on the surface of the liquid metal strongly influenced by the oxide skin on the liquid metal.[30] In the current study, no such dependence on the oxide skin is observed, and it is demonstrated that the interaction at the interface of Ga and thin films like Au and Pt produces these patterns.

When liquid Ga (or Sn) flows over a very thin, microscale, metallic track of Pt or Au, it spontaneously generates periodic patterns in the form of well-defined ripples. The mechanism of ripple formation is studied in detail with a series of experiments, including *in situ* SEM observations and detailed microstructural characterization. The surface tension acting on the liquid and the solid at the flow front is the driving force for the flow, and it dominates over all possible forces, such as gravity, viscous, inertial, etc., involved in the flow.

The EDS analysis performed in STEM shows a complete dissolution of the substrate, thereby exposing it to the non-wetting Ti layer at the bottom and the Pt-rich layer at the top of the ripple surface. The ripple structure forms as the liquid metal flow over a substrate that transitions from the wetting to the non-wetting, with a relatively more stable intermetallic layer formed at the top surface. When this process flow is simulated using COMSOL Multiphysics, the flow of liquid metal over a wetting surface, the growth of the ripple having an asymmetrical shape can be reproduced in the same manner as observed in the experiments.

The developed qualitative model has scope for improvement but captures the essential physics and lays out ground for further study using this phenomenon. Quantitative modeling of this phenomenon can be investigated from a more fundamental perspective as commercially available CFD software lacks it presently. Controlling the ripple patterns with respect to the height, pitch, gap, and type of metal needs investigation that can lead to novel applications like diffraction gratings and parallel microfluidic channels.

■ ASSOCIATED CONTENT

Supporting Information

The Supporting Information is available free of charge at https://pubs.acs.org/doi/10.1021/acsomega.2c00364.

Video S1: Ripple formation at 3000× magnification (MP4)

Video S2: Ripple formation at 12,000× magnification (MP4)

Video S3: Flow on the discontinuous path (MP4)

Video S4: COMSOL simulation capturing asymmetry (MP4)

Video S5: COMSOL simulation capturing splitting (MP4)

Video S6: Ripple formation at 50,000× magnification (MP4)

Video S7: Top surface movement on a non-patterned substrate (MP4)

Document with additional experimental details on ripple formation (PDF)

■ AUTHOR INFORMATION

Corresponding Author

Praveen Kumar − *Department of Materials Engineering, Indian Institute of Science, Bangalore 560012, India;* orcid.org/0000-0002-8890-9969; Email: praveenk@iisc.ac.in

Authors

Vijayendra Shastri − *Center for Nanoscience and Engineering, Indian Institute of Science, Bangalore 560012, India*

Santanu Talukder − *Department of Electrical Engineering and Computer Science, Indian Institute of Science Education and Research, Bhopal 462066, India*

Kaustav Roy − *Center for Nanoscience and Engineering, Indian Institute of Science, Bangalore 560012, India*

https://doi.org/10.1021/acsomega.2c00364
ACS Omega 2022, 7, 12111−12119

Rudra Pratap − *Center for Nanoscience and Engineering, Indian Institute of Science, Bangalore 560012, India*

Complete contact information is available at: https://pubs.acs.org/10.1021/acsomega.2c00364

Notes

The authors declare no competing financial interest.

■ ACKNOWLEDGMENTS

The authors would like to thank Drs. Dipali Sonawane and Esakkiraja Neelamegan of the Indian Institute of Science, Bangalore for helping the lamellae for STEM, Professors Amit Tandon of the University of Massachusetts, Dartmouth, Jason Picardo of the Indian Institute of Technology, Bombay, and Gaurav Tomar of the Indian Institute of Science, Bangalore for insightful discussions. The authors also acknowledge financial support from the Department of Science and Technology (DST), India (grant number DST01526). The authors also thank the staff at the Micro and Nano Characterization Facility (MNCF), National Nanofabrication Center (NNFC), and Advanced Microscopy and Microanalysis (AFMM) at the Indian Institute of Science, Bangalore.

■ ADDITIONAL NOTES

[a]It should be noted that Ga is liquid at room temperature in Bangalore (India), and an external heat is not essential for the flow. However, some external heat can enhance the velocity of the flow of Ga and help manipulate the ripple flow pattern.
[b]The contamination due to the formation of the amorphous layer[31] of Ga is insignificant as compared to the total thickness of lamellae. Hence, Ga implantation due to FIB milling can be ignored.

■ REFERENCES

(1) Ball, P. Pattern Formation in Nature : Physical Constraints and Self-Organising Characteristics. *Archit. Des* **2012**, *82*, 22−27.
(2) Gregg, T. K. P. Patterns and Processes: Subaerial Lava Flow Morphologies: A Review. *J. Volcanol. Geotherm.* **2017**, *342*, 3−12.
(3) Dolgopolova, E. N. The Conditions for Tidal Bore Formation and Its Effect on the Transport of Saline Water at River Mouths. *Water Resour.* **2013**, *40*, 16−30.
(4) Bobb, L. C.; Ferguson, G.; Rankin, M. Capillary Wave Measurements. *Appl. Opt.* **1979**, *18*, 1167.
(5) Yang, J.; Zhou, T.; Zhang, L.; Zhu, D.; Handschuh-Wang, S.; Liu, Z.; Kong, T.; Liu, Y.; Zhang, J.; Zhou, X. Defect-Free, High Resolution Patterning of Liquid Metals Using Reversibly Sealed, Reusable Polydimethylsiloxane Microchannels for Flexible Electronic Applications. *J. Mater. Chem. C* **2017**, *5*, 6790−6797.
(6) Kim, D.; Yoon, Y.; Kauh, S. K.; Lee, J. Towards Sub-Microscale Liquid Metal Patterns: Cascade Phase Change Mediated Pick-n-Place Transfer of Liquid Metals Printed and Stretched over a Flexible Substrate. *Adv. Funct. Mater.* **2018**, *28*, 1800380.
(7) Schleunitz, A.; Schift, H. Fabrication of 3D Nanoimprint Stamps with Continuous Reliefs Using Dose-Modulated Electron Beam Lithography and Thermal Reflow. *J. Micromech. Microeng.* **2010**, *20*, 095002.
(8) Schift, H.; Schleunitz, A. Fabrication of Stepped and Reflowed 3-D Profiles for Optical Applications by Dose-Modulated Electron Beam Lithography and Selective Thermal Reflow. *CLEO - Laser Science to Photonic Applications* **2011**, 1−2.
(9) Talukder, S. Study and Control of Electromigration Driven Material Transport for Applications in Nanofabrication and Patterning. *PhD Thesis, Indian Inst. of Sci.* **2015**.
(10) Shastri, V. Study of Micro-and Nano-Scale Transport of Liquid Metal on Thin Solid Films. *PhD Thesis, Indian Inst. of Sci.* **2021**.
(11) Joshipura, I. D.; Ayers, H. R.; Castillo, G. A.; Ladd, C.; Tabor, C. E.; Adams, J. J.; Dickey, M. D. Patterning and Reversible Actuation of Liquid Gallium Alloys by Preventing Adhesion on Rough Surfaces. *ACS Appl. Mater. Interfaces* **2018**, *10*, 44686−44695.
(12) Li, Q.; Lin, J.; Liu, T.; Dong, S.; Zheng, H.; Liu, J. Supermetallophobic Functional Coatings Based on Silicate Clays and a Method to Pattern Liquid Metals. *ACS Appl. Electron. Mater.* **2020**, *2*, 2229−2241.
(13) Jiang, Y.; Su, S.; Peng, H.; Sing Kwok, H.; Zhou, X.; Chen, S. Selective Wetting/Dewetting for Controllable Patterning of Liquid Metal Electrodes for All-Printed Device Application. *J. Mater. Chem. C* **2017**, *5*, 12378−12383.
(14) Bo, G.; Ren, L.; Xu, X.; Du, Y.; Dou, S. Recent Progress on Liquid Metals and Their Applications. *Adv. Phys.: X* . **2018**, 412−442.
(15) Park, C. W.; Moon, Y. G.; Seong, H.; Jung, S. W.; Oh, J. Y.; Na, B. S.; Park, N. M.; Lee, S. S.; Im, S. G.; Koo, J. B. Photolithography-Based Patterning of Liquid Metal Interconnects for Monolithically Integrated Stretchable Circuits. *ACS Appl. Mater. Interfaces* **2016**, *8*, 15459−15465.
(16) An, L.; Jiang, H.; Branco, D. d. C.; Liu, X.; Xu, J.; Cheng, G. J. Self-Packaged High-Resolution Liquid Metal Nano-Patterns. *Matter* **2022**, *5*, 1016−1030.
(17) Bonn, D.; Eggers, J.; Indekeu, J.; Meunier, J.; Rolley, E. Wetting and Spreading Dynamics. *Plasma Processes Polym.* **2008**, *5*, 206−258.
(18) Saiz, E.; Tomsia, A. P. Atomic Dynamics and Marangoni Films during Liquid-Metal Spreading. *Nat. Mater.* **2004**, *3*, 903−909.
(19) Yunusa, M.; Amador, G. J.; Drotlef, D. M.; Sitti, M. Wrinkling Instability and Adhesion of a Highly Bendable Gallium Oxide Nanofilm Encapsulating a Liquid-Gallium Droplet. *Nano Lett.* **2018**, *18*, 2498−2504.
(20) Yazdanpanah, M. M. Near Room Temperature Self-Assembly of Nanostructures by Reaction of Gallium with Metal Thin Films, PhD Thesis, Univ. of Louisville 2006.
(21) Glickman, E.; Levenshtein, M.; Budic, L.; Eliaz, N. Interaction of Liquid and Solid Gallium with Thin Silver Films: Synchronized Spreading and Penetration. *Acta Mater.* **2011**, *59*, 914−926.
(22) Okamoto, H. Ga-Pt (Gallium-Platinum). *J. Phase Equilib. Diffus.* **2007**, *28*, 11669.
(23) Jendrzejczyk-Handzlik, D. Thermodynamic Study and Re-Optimization of the Au-Ga Binary System. *J. Phase Equilib. Diffus.* **2017**, *38*, 305−318.
(24) Mugele, F.; Heikenfeld, J. Introduction to Capillarity and Wetting Phenomena. *In Electrowetting: Fundamental Principles and Practical Applications*; 1st ed.; Wiley-VCH Verlag GmbH 2018; pp. 1−59, DOI: 10.1002/9783527412396.ch1.
(25) Spells, K. E. The Determination of the Viscosity of Liquid Gallium over an Extended Range of Temperature. *Proc. Phys. Soc.* **1936**, *48*, 299−311.
(26) Abbaschian, G. J. Surface Tension of Liquid Gallium. *J. Less-Common Met.* **1975**, *40*, 329−333.
(27) de Gennes, P.G.; Brochard-Wyart, F.; Quere, D.; *Capillarity and Wetting Phenomena.* Translated by Reisinger .A.; Springer New York 2004.
(28) White, F. M. *Fluid Mechanics*; McGrawHill-New York, 1979
(29) Eid, K. F.; Panth, M.; Sommers, A. D. The Physics of Water Droplets on Surfaces: Exploring the Effects of Roughness and Surface Chemistry. *Eur. J. Phys.* **2018**, *39*, 025804.
(30) Tang, J.; Lambie, S.; Meftahi, N.; Christofferson, A. J.; Yang, J.; Ghasemian, M. B.; Han, J.; Allioux, F. M.; Rahim, M. A.; Mayyas, M.; Daeneke, T.; McConville, C. F.; Steenbergen, K. G.; Kaner, R. B.; Russo, S. P.; Gaston, N.; Kalantar-Zadeh, K. Unique Surface Patterns Emerging during Solidification of Liquid Metal Alloys. *Nat. Nanotechnol.* **2021**, *16*, 431−439.
(31) Yabuuchi, Y.; Tametou, S.; Okano, T.; Inazato, S.; Sadayama, S.; Yamamoto, Y.; Iwasaki, K.; Sugiyama, Y. A Study of the Damage on FIB-Prepared TEM Samples of AlxGa 1-XAs. *J. Electron Microsc.* **2004**, *53*, 471−477.